Activated carbon from residual oil fly ash for heavy metals removal from aqueous solution

Sirajus Salehin[a], Asad S. Aburizaiza[a,b], M.A. Barakat[a,b,]*

[a]Faculty of Meteorology, Environment and Arid Land Agriculture, Department of Environmental Sciences, King Abdulaziz University, Jeddah 21589, Saudi Arabia, emails: sirajussalehin@yahoo.com (S. Salehin), asad_ziz@yahoo.com (A.S. Aburizaiza), Tel. +966 02 6400000/64821; email: mabarakat@gmail.com (M.A. Barakat)
[b]Center of Excellence in Environmental Studies (CEES), King Abdulaziz University, Jeddah, Saudi Arabia

ABSTRACT

This study investigated the potentiality of residual oil fly ash as a precursor of activated carbon (AC). Fly ash samples were activated by physical activation method, i.e. with CO_2 flow at 950℃ for 2 h. Samples were characterized by BET, SEM, FTIR, and XRD techniques. The produced AC developed a high surface area (269.013 m^2/g). The synthesized AC was then examined as an adsorbent for Cu(II) and Pb(II) removal from aqueous solutions. The effect of solution pH, initial solution concentration, and contact time were studied. Results of batch experiments for precipitation (in absence of AC) showed that removal of both Cu(II) and Pb(II) ions by precipitation was occurred at pH 6 and increased at pH 7 with removal values of 52.5 and 88.1%, respectively. On another hand, higher removal efficiency of metal ions by adsorption (in presence of AC) was achieved with increased solution pH levels. Adsorption values of 72.7 and 78.5% were achieved at pH 5 for Cu(II) and Pb(II), respectively. Complete removal (99 and 99.3% for copper and lead, respectively) of both metals was achieved at pH 7 (adsorption and precipitation). The maximum equilibrium time of adsorption was found to be 30 min for the two metal ions. Kinetics studies revealed that the adsorption of Cu(II) and Pb(II) onto AC followed the pseudo-second-order kinetics and the adsorption equilibrium data were well fitted to Langmuir isotherm model.

Keywords: ROFA; Oil fly ash; Activated carbon; CO_2 activation; Heavy metals adsorption; Cu(II) and Pb(II) removal

1. Introduction

Residual oil fly ash (ROFA) is the solid residue that is produced when residual fuel oil is burnt extensively. This fuel oil is obtained from the crude petroleum after several stages of refining. In Saudi Arabia, residual fuel oil is abundantly used in power generation and desalination industries which results in the generation of a huge amount of ROFA annually. It is rich in carbonaceous matter (amount varies from 64 to 97 wt.%) which has been determined through loss of ignition technique in previous studies [1,2]. It

*Corresponding author.

has been found that ROFA particles are composed of organic sulfur (S) molecules along with several inorganic chemical elements such as vanadium (V), nickel (Ni), iron (Fe), and zinc (Zn) in any of the forms of sulfates, oxides, vanadates, and phosphates [1]. Since it cannot be used in cement industries like coal burned fly ash due to its higher carbon concentrations, the end use of ROFA is to be dumped in the landfills which is hazardous to the environment in many ways [3,4]. Therefore, finding a proper usage of ROFA is a pressing matter in this country. Many studies have been done so far regarding the preparation of activated carbon (AC) from different types of fly ash such as heavy oil fly ash [5,6], coal burned fly ash [7–10], and bagasse fly ash [11,12].

Basically, there are two methods of preparing AC, namely physical and chemical activation. Physical activation starts with the carbonization of the sample (under 700°C) followed by the controlled flow of oxidizing agents such as steam, carbon dioxide, or both together at higher temperature (upto 1,100°C). These oxidizing agents initiate a heterogeneous reaction on the carbon surface of the sample which includes the transportation of gaseous molecules and their diffusion and thus, helping to develop better surface area and microporosity [13]. On the other hand, chemical activation incorporates the uses of chemical agents such as KOH, $ZnCl_2$, H_3PO_4, etc. which deter the formation of tar during the reaction as well as restrict the development of volatile matters and thus suppress the shrinking of the precursor molecules. And when the chemicals are removed through the heating of the sample, internal porosity is developed greatly [13,14].

Physical activation via either steam [7–10] or CO_2 [5,6,13,15] was found emphatic in the mentioned studies. However, recently it has been proven that chemical activation alone or a combined activation method using any of the chemical agents stated earlier and CO_2 together which is also known as physicochemical activation could produce AC with better surface area and adsorption capacity [11,12].

Throughout the past few decades, AC has been the most desired adsorbent of heavy metals from aqueous solution. Among the studied metals in previous research works Ni, Cr, Pb, As, Cu, Cd, and Hg were considered mostly for AC adsorption experiments where the precursors of AC came from a wide variety of sources except ROFA such as bamboo [16,17], cow bone [18], cashew nuts [19], coconut shell [17,20], hazelnut husks [21], tamarind seeds [22], grape seeds [23], apricot seeds [24], tobacco waste [25], pine and eucalyptus wood [17], mineral bituminous and lignite charcoal [17], plum kernel, and jacaranda biomass [26].

Considering the waste management scenario in Saudi Arabia, this study is quite significant since ROFA volume is increasing gradually and it has no potential use. Besides, there are no such previous studies regarding the conversion of ROFA into AC. Therefore, the aim of this study is to prepare AC utilizing ROFA and characterize it for understanding the extent and effect of the activation method applied, and finally using this AC for Cu(II) and Pb(II) removal from aqueous solution.

2. Material and methods

2.1. Preparation of AC from ROFA

ROFA sample has been collected from Rabeigh power plant in Rabeigh, Saudi Arabia. Initially, acid leaching with 1 M HCl solution was conducted to the selected samples in room temperature where the solid–liquid ratio (g/ml) was 1:20 and the mixing duration was 17 h. Then, the solution was filtered and washed several times with deionized water. This was done to remove the metal contents from the samples (detailed study was done separately), and to get concentrated carbon for the experiment. After that, the samples were dried in oven at 105°C for 24 h and kept in the desiccator prior to activation.

Samples were activated using CO_2 gas as an activating agent in a horizontal tube furnace (GSL-1800S60, MTI Inc.). The activation temperature was set at 950°C and kept for 2 h. Around 5 g of sample was put in a crucible and then placed inside the tube. A raw (unactivated) ash sample was also considered for this study to compare the changes occurred due to this physical activation method. The furnace heating rate and CO_2 pressure were maintained at 5°C min^{-1} and 6 ψ (pounds per square inch), respectively.

2.2. Characterization of the AC samples

Multipoint BET surface area measurements were performed to get an overview of the porous characteristics of the activated sample such as surface area, pore volume, and pore size distribution. N_2 adsorption isotherm was produced at 77 K for this purpose using Quantachrome Surface Area Analyzer equipment, NOVA 2200e.

FTIR spectroscopy was employed to the samples before and after activation. This technique was used to reveal the presence or absence of certain chemical

functional groups in the samples. Transmission mode was chosen for the FTIR spectra with a frequency range between $4,000–500\,cm^{-1}$ with the aid of Bruker Alpha-E spectrometer.

Scanning electron microscope (SEM) technique was used to observe the qualitative features and the surface topography of studied samples at various magnifications using JEOL scanning electron microscope (JSM-6360 LV).

XRD spectroscopy method was applied to determine the crystalline phases or textures of the studied samples. Rigaku (Ultima IV) multipurpose X-ray diffractometer was used for this purpose. XRD profile of the activated sample was achieved using Bragg's Eq. (9) at 2θ range from 20° to 80°.

2.3. Adsorption of heavy metals on the AC samples

Batch adsorption experiments were conducted on synthetic solutions of Cu^{2+} and Pb^{2+} using standard salts of $CuCl_2 \cdot 2H_2O$ and $Pb(NO_3)_2$. Effect of time (till 1 h), pH (3–7), and concentration (10, 25, 50, 75, 100 ppm) were examined throughout the entire study while the adsorbent dose was invariant (0.5 g/l) at all times. It needs to be mentioned that the batch adsorption experiment was designed and conducted up to 4 h, but after first 60 min there was no change in adsorption behavior. Hence, all the adsorption experiments were performed up to 1 h.

Erlenmeyer flasks of 250 ml were used for all the experiments and put on a magnetic stirrer. Samples were taken in different time intervals up to 60 min. At each time interval, 5 ml of samples were taken using standard calibrated pipette, filtered immediately, and then the filtrate was diluted up to 50 ml. Then, the remaining Cu^{2+} and Pb^{2+} ions in the solutions were analyzed by UV–visible spectrophotometer (HACH, Lange DR6000). Chemical complex agents were used for each analysis such as LCK-(306) for lead at 520 nm, and powder pillows with bicinchoninate method for copper at 560 nm.

The removal efficiency was calculated using the following Eq. (1) [21]:

$$\% \text{ Removal} = \frac{C_0 - C_e}{C_0} \times 100 \qquad (1)$$

where C_0 and C_e denote the initial and equilibrium concentrations of the adsorbates, individually.

For all dilutions, deionized water was used (Millipore, Elix) and the pH was adjusted using 0.1 M solutions of HCl and NaOH.

3. Results and discussion

3.1. Characterization of AC sample

3.1.1. BET surface area analysis

BET analysis was performed and the specific surface area values for both raw ash and CO_2 activated ash samples were 110.88 and 269.01 m^2/g, respectively. The increase in surface area was approximately 2.5 times more due to CO_2 activation. In addition, the micropore volume (0.07 cc/g, after activation) was broadened during the treatment (Table 1). The prepared AC sample has got both micropores (<2 nm) and mesopores (2–50 nm) that are classified by International Union of Pure and Applied Chemistry (IUPAC) [27]. But, the micropore volume was found greater than the mesopore volume which resembles the findings of a recent study [28].

3.1.2. SEM analysis

The studied ROFA samples were investigated with scanning electron microscopy to find out the morphological features of the raw ash and changes done during the CO_2 activation. Both the raw ash and AC samples were black and powdery that corresponds with earlier studies [29]. SEM micrographs of studied samples are shown in Fig. 1(a)–(d) where the samples appeared as cenospheres (Fig. 1(a) and (c)) [6,29] or porous globular particles [30,31] (Fig. 1(b) and (d)). The particle size ranged from very minute to as high as 100 μm that is relevant to another study [30]. The presence of various broken particles is also noticeable. Fig. 1(a)–(b) depicts the raw sample (before activation) with two different magnifications. It is seen that the raw sample possessed a jagged surface structure (Fig. 1(b)).

CO_2 activation enhanced the porous characteristics of the particles to a moderate extent (from 110.9 to 269.013 m^2/g) and particles with quite smooth outer surface have been produced (Fig. 1(d)). Such kind of appearance was mentioned in a previous study [29]. The development of porosity is better understood in (Fig. 1(d)), i.e. the broadening of pores as discussed in Section 3.1. From the morphological presentations of the samples, it can be inferred that the gasification was implemented involving the total mass of the cenospheres [4].

3.1.3. FTIR analysis

FTIR spectra of both raw and CO_2 activated ash samples are shown in Fig. 2. In the raw ash sample, the only noticeable peak was found at $1,746\,cm^{-1}$

Table 1
BET surface area and pore volume obtained for Rabeigh ROFA samples

Experimental conditions	Weight loss (%)	Surface area (m^2/g)	Pore volume (cc/g)	
			Micropore (<2 nm)	Mesopore (2–50 nm)
Raw ash	None	110.887	0.043	None
CO_2 activated ash (950℃/2 h)	16.67	269.013	0.07	0.02
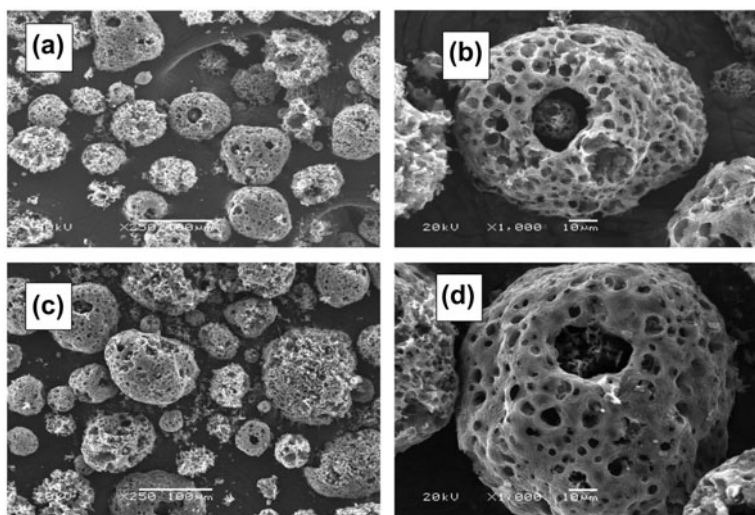
Fig. 1. SEM micrographs of Rabeigh ROFA samples: (a–b) raw ash; (c–d) CO_2 activated ash (950℃/2 h).
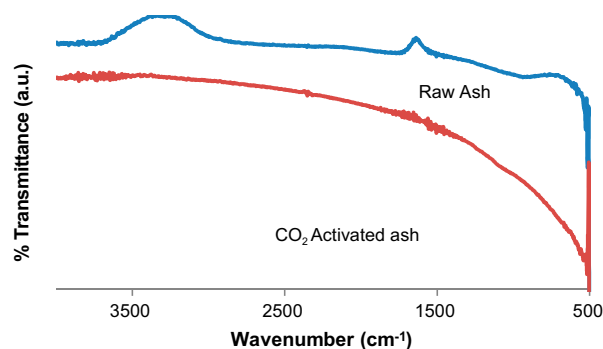
Fig. 2. FTIR spectra of Rabeigh ROFA samples.

On the other hand, CO_2 activated sample shows extremely minor undulations at several regions such as 516–562, 1,470–1,568, 1,651–1,694, 1,714–1,731, and 3,607–3,687 cm^{-1}. The peak at 1,504 cm^{-1} actually depicts the functional group of aromatic C=C which was found at 1,467 cm^{-1} by Shawabkeh et al. [30]. The peak at 3,687 cm^{-1} is possible because of stretched –O–H bond and was mentioned in previous studies where the authors observed this peak at 3,650 cm^{-1} [30,35]. The presence of C=O which is in the ester group

which was due to diketones (C=O) and was reported in several studies at different ranges such as at 1,720, 1,760, and 1,623 cm^{-1} [30–32]. Besides this, there were several minor peaks observed in the region of 513–596 cm^{-1}. The peaks closer to 560 cm^{-1} indicate the existence of Al in aluminosilicates like mullite which was reported elsewhere [33], whereas the peaks near 516 cm^{-1} show the presence of C–C group in alkane [34].

Fig. 3. XRD patterns of Rabeigh ROFA samples.

was found in the region of 1,650–1,731 cm^{-1} that was cited in a study in the range of 1,720–1,760 cm^{-1} [30].

3.1.4. XRD analysis

XRD patterns of the raw ash and CO_2 activated ash samples are illustrated in Fig. 3. In both samples, similar type of broad peaks evolved, which were reflected from the planes. These broad peaks reveal the highly disordered and amorphous nature of ACs that were dealt with in this experiment. This behavior might be due to the acid treatment that was discussed before which completely removed the peaks associated with the ash [9].

In general, the alike broad diffractions at (0 0 2) plane in every sample match with graphitic reflections near $26° = 2\theta$ and it suggests a particular graphitic array in the molecular planes along with the presence of mullite which was mentioned in previous studies [31,36]. In addition, minor broad peaks were also seen closer to $43° = 2\theta$ which indicates the existence of mullite or sodalite [30].

However, the interlayer space (d) varied from 3.489 to 3.507 Å in studied samples which were larger than the graphite (3.354 Å). It implies all the prepared samples had carbonaceous structure [37]. Besides, the negligibility of crystalline phases in the samples fits in with carbonaceous and porous particles which were again supported by SEM study and this phenomenon was described elsewhere [38].

3.2. Adsorption of heavy metals on the AC samples

3.2.1. Effect of initial pH

Batch adsorption experiments were conducted for adsorption of Cu^{2+} and Pb^{2+} on the synthesized AC samples. The effect of initial pH of the solution on adsorption is very dynamic as it is directly involved in altering the surface charge of the adsorbent [21,39], which could be influential determining the adsorption efficiency. Therefore, five different pH ranges (3–7) were studied to select the optimum one that could adsorb the two heavy metals of interest at the highest level. Fig. 4 depicts the rate of adsorption with increasing pH levels.

For both metals, the adsorption efficiency increased with the increase in the initial pH. Reduced adsorption phenomena were observed at lower pH levels such as 3 and 4 for both Cu(II) and Pb(II) which was 45.1–65.6 and 38.9–57.3%, respectively. This is due to the protonation that occurs at the active sites of the adsorbent which restricts the spontaneous uptake of the metal ions present in the solution [34,39]. At pH 5, the adsorption efficiency for Cu(II) and Pb(II) was found to be 72.7 and 78.5% respectively. The maximum removal of Cu(II) and Pb(II) was achieved at pH 6 and 7 which was 98.6–99 and 92.1–99.3%, respectively. But precipitation of both metals took place at those levels of pH as insoluble metal hydroxides, thus the metal removal at such pH is a combination between precipitation and adsorption [21]. For this, a separate experiment was conducted to find out the precipitation behavior of the studied metals under the current experimental conditions. That experiment revealed that both the Cu(II) and Pb(II) ions did not precipitate until pH 5. But at pH 6 and 7, the rate of precipitation was 39–52.5% for Cu(II) and 60.7–88.1% for Pb(II) (Fig. 4). Hence, pH 5 was considered as the optimum pH for adsorption of the studied metals in this experiment and used for later experiments.
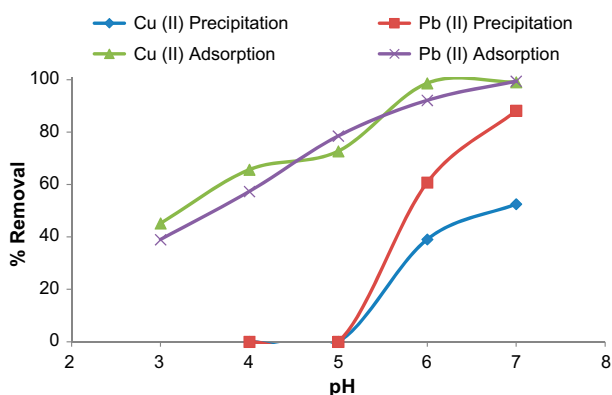
Fig. 4. Effect of initial pH on Cu(II) and Pb(II) adsorption and precipitation (adsorbent dose 0.5 g/l, contact time 60 min, and initial metals concentration 25 ppm).
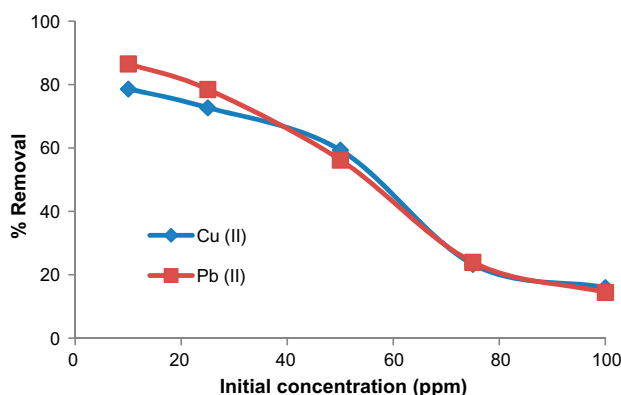
Fig. 5. Effect of initial metals concentrations on Cu(II) and Pb(II) adsorption (adsorbent dose 0.5 g/l, pH 5, and contact time 60 min).

3.2.2. Effect of initial metals concentration

The effect of initial metal concentrations on the adsorption efficiency of Cu(II) and Pb(II) is presented in Fig. 5. It is clear that the percentage of adsorption increased as the initial metals' concentrations were decreased. The adsorption efficiency values were 78.6, 72.7, 59.3, 23.3, and 16% for Cu(II), while the values were 86.5, 78.5, 56.2, 24, and 14.5% for Pb(II) with initial metals concentration of 10, 25, 50, 75, and 100 ppm, respectively. A previous study mentioned about enough vacant adsorption sites at lower metals concentrations, whereas at higher concentrations, the number of metal ions become abundant than the adsorption sites and hence, the reduced adsorption efficiency [21]. Therefore, it could be inferred that the adsorption of both Cu(II) and Pb(II) was extremely concentration reliant and with lower initial concentrations, Pb(II) could be removed more efficiently than Cu(II).

3.2.3. Effect of contact time

Fig. 6 illustrates the effect of contact time on adsorption of both Cu(II) and Pb(II) up to 1 h. It is seen that the adsorption took place within short time for both metals. The equilibrium of adsorption has been established in 30 min. The reason behind high initial adsorption with celerity is due to the active adsorption sites which outnumber the metal ions present in the solution. It again relates the adsorption mechanism with the concentration of metal ions. This behavior follows the findings of previous studies [21,34]. At equilibrium phase, the adsorption of Cu(II) and Pb(II) was found as 72.7 and 78.5%, respectively, which demonstrates higher Pb(II) removal rate than Cu(II).
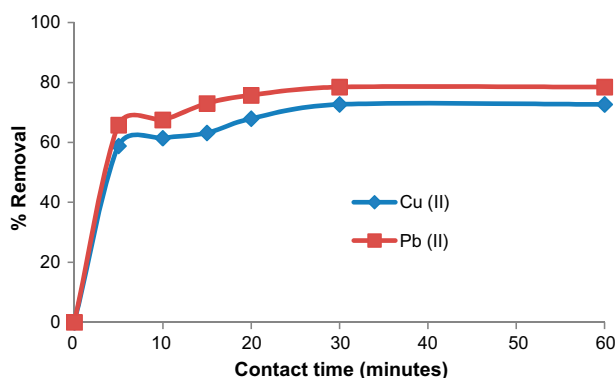
Fig. 6. The effect of contact time on adsorption of Cu(II) and Pb(II) (adsorbent dose 0.5 g/l, pH 5, and initial concentration 25 ppm).

3.3. Adsorption isotherm models

In any adsorption system, adsorption isotherms are of immense importance to find out the correlations between adsorbate and adsorbent at equilibrium conditions. There are several models with distinguished parameters which facilitate to understand the adsorption mechanism, behavior of the adsorbent surface during adsorption, and its capacity to adsorb in certain experimental circumstances upon the fitness to each of these models [37].

This study investigated two adsorption isotherm models that are widely used, Langmuir [Eq. (2)] and Freundlich [Eq. (3)] models [18]:

$$\frac{C_e}{q_e} = \frac{1}{K_L \times q_m} + \frac{C_e}{q_m} \tag{2}$$

$$\ln q_e = \ln K_F + \frac{1}{n} \times \ln C_e \tag{3}$$

For Langmuir model, K_L is the Langmuir constant for adsorption (L/mg) and q_m indicates theoretical maximum adsorption capacity (mg/g). In the other model, K_F represents the Freundlich constant of adsorption capacity (mg/g (L/mg)$^{1/n}$) and n denotes the favorability of adsorption process or adsorption intensity, in other words. The interpretation with the n value is done as: $n < 1$ (poor), $1 < n < 2$ (medium/with difficulties), and $2 < n < 10$ (favorable/spontaneous) [37]. The calculated parameters of both Langmuir and Freundlich models are presented in Table 2.

It is clearly seen that the studied adsorption process fitted well with the Langmuir model (Fig. 7) ($r^2 > 0.988$ (Cu^{2+}) and $r^2 > 0.980$ (Pb^{2+})). It implies that the adsorption was homogenous and occurred in a monolayer [37,40]. Cechinel et al. [18] also added a feature to this model that a chemical reaction occurs primarily that binds the adsorbates onto the surface of the adsorbent and all the sites have same attraction to the adsorbates.

On the other hand, though the experimental adsorption did not fit with the Freundlich model (Fig. 8), the n value (5.21 for Cu^{2+}, 7.56 for Pb^{2+}) suggests that the adsorption underwent quite spontaneously and the intensity was higher for Pb^{2+} than Cu^{2+}.

3.4. Adsorption kinetics models

Usually in liquid–solid adsorption systems, the mass transfer of a solute takes place from the aqueous phase to the external surface of the adsorbent [41]. Thus, the study of adsorption kinetics is very useful to

Table 2
Values of Langmuir and Freundlich constants for Cu(II) and Pb(II) adsorption isotherms

Adsorbates	Langmuir constants			Freundlich constants		
	K_L (L/mg)	q_m (mg/g)	r^2 (corr. coeff.)	K_F (mg/g (L/mg)$^{1/n}$)	n	r^2 (corr. coeff.)
Cu(II)	−0.703	32.47	0.9885	18.06	5.21	0.3919
Pb(II)	−0.377	29.85	0.9806	21.87	7.56	0.3182
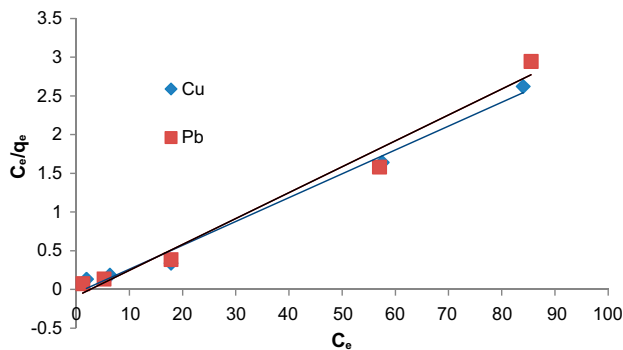
Fig. 7. Langmuir model for Pb^{2+} and Cu^{2+} adsorption isotherm.
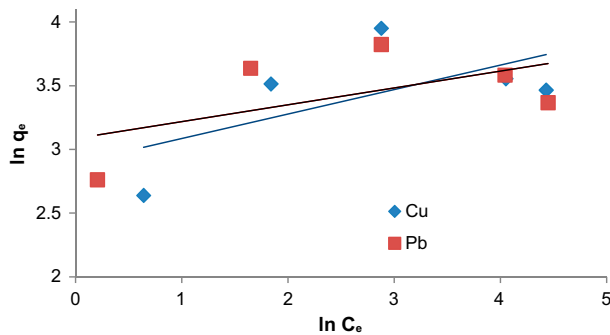
Fig. 8. Freundlich model for Pb^{2+} and Cu^{2+} adsorption isotherm.

understand the adsorption mechanism which describes the efficiency of the adsorption system [41], and determining sorption rates with characteristics of possible reaction mechanism [42]. Therefore, the pseudo-first-order kinetics model, pseudo-second-order kinetics model and intraparticle diffusion model were used in this study to test the obtained experimental data.

3.4.1. Pseudo-first-order kinetics model

The most widely known Lagergren adsorption rate expression was used to describe pseudo-first-order kinetics model [41] and is shown below in Eq. (4):

$$\log (q_e - q_t) = \log q_e - \frac{k_{pf} \times t}{2.303} \tag{4}$$

where q_e represents the amount adsorbed (mg/g) at equilibrium phase, q_t denotes the amount adsorbed (mg/g) at time t, and k_{pf} refers to the adsorption rate constant (min^{-1}). The values of these parameters are shown in Table 3. The derived plot of $\log (q_e - q_t)$ vs. t using Eq. (1) is presented in Fig. 9. The k_{pf} values for Cu(II) and Pb(II) were 0.06 and 0.1 min^{-1}, respectively. The correlation-coefficient (r^2) values are higher in Pb(II) (0.94) than found in Cu(II) (0.88). Besides, the equilibrium adsorption (q_e) for Cu(II) and Pb(II) were severally 9.84 and 12.30 mg/g which is far beyond the experimental equilibrium adsorption ($q_{e,exp}$) that was 33.6 and 38 mg/g for Cu(II) and Pb(II), respectively. In this respect, it can be said that the studied adsorption system did not follow pseudo-first-order kinetics model.

3.4.2. Pseudo-second-order kinetics model

On the other hand, it has been reported that most adsorption system fits well with the pseudo-second-order kinetics model [41]. This model assumes chemisorption as the rate-limiting factor that is the adsorption process takes place due to physicochemical interactions between solid and liquid phases [42].

This model can be expressed with the Eq. (5) [41]:

$$\frac{t}{q_t} = \frac{1}{k_{ps} \times q_e^2} + \frac{t}{q_e} \tag{5}$$

where k_{ps} refers to the adsorption rate constant (g/(mg.min)). The k_{ps} values were calculated using the plots of t/q_t vs. time (Fig. 10), and the linear correlation coefficient (r^2) values were obtained from the slopes of the plots. It was found (Table 3) that the correlation coefficient (r^2) values were close to 1 (Cu^{2+}: 0.995; Pb^{2+}: 0.997), proposing the best fit of this kinetics equation and the characteristic pseudo-second-order mechanism for removing Cu(II) and Pb(II)

Table 3
Adsorption kinetics parameters of Cu(II) and Pb(II) on activated carbon

HMI	EAC, $q_{e(exp)}$ (mg/g)	Pseudo-first-order kinetic model			Pseudo-second-order kinetic model			Intraparticle diffusion model		
		k_{pf} (min^{-1})	q_e (mg/g)	r_1^2	k_{ps} (g/(mg min))	q_e (mg/g)	r_2^2	k_{id} (mg/g min$^{1/2}$)	C_i	r^2
Cu^{2+}	33.6	0.06	9.84	0.88	0.022	32.89	0.995	1.28	24.79	0.839
Pb^{2+}	38	0.10	12.30	0.94	0.0177	38.91	0.997	1.20	30.03	0.776

Notes: HMI: heavy metal ions; EAC: experimental adsorption capacity.
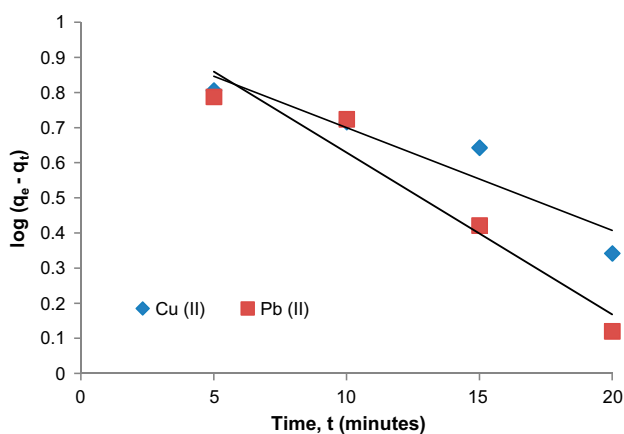
Fig. 9. Pseudo-first-order kinetics model for Cu(II) and Pb (II) ions adsorption on activated carbon from ROFA.
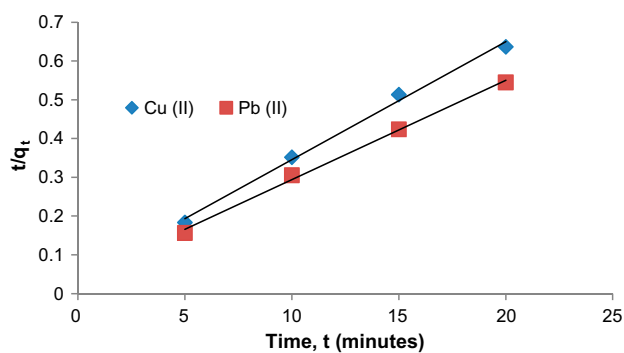
Fig. 10. Pseudo-second-order kinetics model for Cu(II) and Pb(II) ions adsorption on activated carbon from ROFA.

ions onto ROFA AC. In addition, the equilibrium adsorption (q_e) values were well described with the experimental equilibrium adsorption ($q_{e,exp}$) such as 32.89 (q_e) vs. 33.6 ($q_{e,exp}$) mg/g, for Cu(II) ions and 38.91 (q_e) vs. 38 ($q_{e,exp}$) mg/g, for Pb(II) ions. Hence, it can be deduced that the examined adsorption system

followed the pseudo-second-order kinetics model. Similar findings were reported in previous studies [41] with different kind of adsorbent.

3.4.3. Intraparticle diffusion model

The intraparticle diffusion model specifies the transportation mechanism of the adsorbates into the adsorbents in a solution which often might be a rate-limiting step in any adsorption system [41]. The rate constant of intraparticular diffusion model can be calculated from the following Eq. (6) that was developed by Weber Morris [41]:

$$q_t = k_{id} \times t^{0.5} + C_i \tag{6}$$

where k_{id} denotes the diffusion coefficient (mg/g.min$^{1/2}$) and q_t indicates the amount adsorbed (mg/g) at time t (min). The values of these parameters were presented in Table 3. Plots of q_t vs. $t^{1/2}$ are presented in Fig. 11 for the studied heavy metal ions. The intercept (C_i) values were calculated from the slope equations. It was found that both the plots followed a similar 3-phased pattern that is a curved portion at
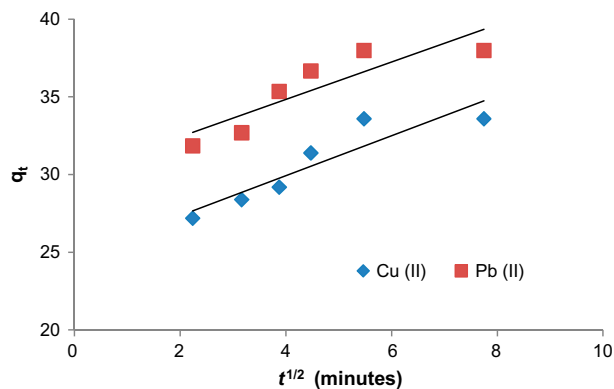
Fig. 11. Intraparticular diffusion model for Cu(II) and Pb(II) adsorption onto ROFA activated carbon.

the beginning, a linear portion at the middle, and a flat plateau at the end. The initial curved portion refers to the bulk or film diffusion of the studied metal ions. At the second phase, the metals adsorption rate increased sharply as the internal or pore diffusion is assumed to be taken place there where the adsorbates transported to the internal active sites through the pores. Finally, the plateau describes the equilibrium stage of adsorption when the diffusion rates for both the metals started to slow down because of the exhaustion of the pore volumes. Almost similar results were found elsewhere [41]. Besides, the deflection in the curves confirms that the intraparticular diffusion is not the only rate-limiting step in the overall adsorption mechanism [41].

The rate constant (k_{id}) values for Cu(II) and Pb(II) ions were found as 1.28 and 1.20 (mg/g.min$^{1/2}$), respectively. From the linear equation, the intercept (C_i) values were also obtained which is proportionally related to the boundary layer thickness [41]. From this relation, it can be said that the boundary layer effect was higher in Pb(II) ions (30.03) than Cu(II) ions (24.79). And the linear correlation coefficient values were 0.839 and 0.776 for Cu(II) and Pb(II), respectively.

4. Conclusion

This study has explored the suitability of ROFA to prepare AC as low-cost adsorbent to remove heavy metals from wastewater. The fly ash samples were successfully activated with CO_2 flow at 950℃ for 2 h. The produced AC was characterized by a high surface area (269.013 m^2/g). The metal adsorption efficiency on the AC was found to be 72.7 and 78.51% for Cu(II) and Pb(II), respectively, at optimum pH 5 after 30 min. Kinetics studies revealed that the adsorption of Cu(II) and Pb(II) onto AC followed the pseudo-second-order kinetics and the adsorption equilibrium data were well fitted to Langmuir isotherm model.

Acknowledgments

Nomenclature

C_0　　— 　initial concentration of the adsorbates
C_e　　— 　equilibrium concentration of the adsorbates
C_i　　— 　the intercept value for intraparticle *diffusion*
n　　　— 　the favorability of adsorption process
r^2　　— 　correlation coefficient
q_m　　— 　theoretical maximum adsorption capacity
q_e　　— 　the amount adsorbed at equilibrium phase
$q_{e\ (exp)}$　— 　experimental adsorption capacity at equilibrium phase
q_t　　— 　the amount adsorbed at time t
K_L　　— 　Langmuir constant for adsorption
K_F　　— 　Freundlich constant of adsorption capacity
k_{pf}　　— 　adsorption rate constant for pseudo-first-order kinetics
k_{ps}　　— 　adsorption rate constant for pseudo-second-order kinetics
k_{id}　　— 　intraparticle diffusion coefficient

References

[1] Y. Chen, N. Shah, F.E. Huggins, G.P. Huffman, Investigation of the microcharacteristics of PM$_{2.5}$ in residual oil fly ash by analytical transmission electron microscopy, Environ. Sci. Technol. 38 (2004) 6553–6560.

[2] G.P. Huffman, F.E. Huggins, N. Shah, R. Huggins, W.P. Linak, C.A. Miller, R.J. Pugmire, H.L.C. Meuzelaar, M.S. Seehra, A. Mannivannan, Characterization of fine particulate matter produced by combustion of residual fuel oil, J. Air Waste Manage. Assoc. 50 (2000) 1106–1114.

[3] M.A. Uddin, Y. Shinozaki, N. Furusawa, T. Yamada, Y. Yamaji, E. Sasaoka, Preparation of activated carbon from asphalt and heavy oil fly ash and coal fly ash by pyrolysis, J. Anal. Appl. Pyrolysis 78 (2007) 337–342.

[4] P. Caramuscio, L.D. Stefano, M. Seggiani, S. Vitolo, P. Narducci, Preparation of activated carbons from heavy-oil fly ashes, Waste Manage. 23 (2003) 345–351.

[5] P. Davini, Flue gas treatment by activated carbon obtained from oil-fired fly ash, Carbon 40 (2002) 1973–1979.

[6] M. Seggiani, S. Vitolo, P.D. Filippis, Effect of pre-oxidation on the porosity development in a heavy oil fly ash by CO_2 activation, Fuel 84 (2005) 1854–1857.

[7] M.T. Izquierdo, B. Rubio, Carbon-enriched coal fly ash as a precursor of activated carbons for SO_2 removal, J. Hazard. Mater. 155 (2008) 199–205.

[8] M.M. Maroto-Valer, Z. Lu, Y. Zhang, Z. Tang, Sorbents for CO_2 capture from high carbon fly ashes, Waste Manage. 28 (2008) 2320–2328.

[9] Z. Lu, M.M. Maroto-Valer, H.H. Schobert, Role of active sites in the steam activation of high unburned carbon fly ashes, Fuel 87 (2008) 2598–2605.

[10] Z. Lu, M.M. Maroto-Valer, H.H. Schobert, Catalytic effects of inorganic compounds on the development of surface areas of fly ash carbon during steam activation, Fuel 89 (2010) 3436–3441.

[11] C.W. Purnomo, C. Salim, H. Hinode, Preparation and characterization of activated carbon from bagasse fly ash, J. Anal. Appl. Pyrolysis 91 (2011) 257–262.

[12] C.W. Purnomo, C. Salim, H. Hinode, Effect of the activation method on the properties and adsorption behavior of bagasse fly ash-based activated carbon, Fuel Process. Technol. 102 (2012) 132–139.

[13] M.L. Sekirifa, M. Hadj-Mahammed, S. Pallier, L. Baameur, D. Richard, A.H. Al-Dujaili, Preparation and

characterization of an activated carbon from a date stones variety by physical activation with carbon dioxide, J. Anal. Appl. Pyrolysis 99 (2013) 155–160.

[14] F. Rodriguez-Reinoso, M. Molina-Sabio, Activated carbons from lignocellulosic materials by chemical and/or physical activation: An overview, Carbon 30 (1992) 1111–1118.

[15] A. Esfandiari, T. Kaghazchi, M. Soleimani, Preparation and evaluation of activated carbons obtained by physical activation of polyethyleneterephthalate (PET) wastes, J. Taiwan Inst. Chem. Eng. 43 (2012) 631–637.

[16] S.F. Lo, S.Y. Wang, M.J. Tsai, L.D. Lin, Adsorption capacity and removal efficiency of heavy metal ions by moso and ma bamboo activated carbons, Chem. Eng. Res. Des. 90 (2012) 1397–1406.

[17] S.D.L. Liliane, S.P. Quinaia, F.L. Melquiadez, G.E.V. de Biasi, J.R. Garcia, Characterization of activated carbons from different sources and the simultaneous adsorption of Cu, Cr, and Zn from metallurgic effluent, Sep. Purif. Technol. 122 (2014) 421–430.

[18] M.A.P. Cechinel, S.M.A.G.U. de Souza, A.A.U. de Souza, Study of lead (II) adsorption onto activated carbon originating from cow bone, J. Cleaner Prod. (2013) 1–8.

[19] P. SenthilKumar, S. Ramalingam, R.V. Abhinaya, S. Dinesh Kirupha, T. Vidhyadevi, S. Sivanesan, Adsorption equilibrium, thermodynamics, kinetics, mechanism and process design of zinc (II) ions onto cashew nut shell, Can. J. Chem. Eng. 90 (2012) 973–982.

[20] X. Song, H. Liu, L. Cheng, Y. Qu, Surface modification of coconut-based activated carbon by liquid-phase oxidation and its effects on lead ion adsorption, Desalination 255 (2010) 78–83.

[21] M. Imamoglu, O. Tekir, Removal of copper (II) and lead (II) ions from aqueous solutions by adsorption on activated carbon from a new precursor hazelnut husks, Desalination 228 (2008) 108–113.

[22] J. Acharya, J.N. Sahu, C.R. Mohanty, B.C. Meikap, Removal of lead (II) from wastewater by activated carbon developed from tamarind wood by zinc chloride activation, Chem. Eng. J. 149 (2009) 249–262.

[23] M. Al Bahri, L. Calvo, M.A. Gilarranz, J.J. Rodriguez, Activated carbon from grape seeds upon chemical activation with phosphoric acid: Application to the adsorption of diuron from water, Chem. Eng. J. 203 (2012) 348–356.

[24] M. Kobya, E. Demirbas, E. Senturk, M. Ince, Adsorption of heavy metal ions from aqueous solutions by activated carbon prepared from apricot stone, Bioresour. Technol. 96 (2005) 1518–1521.

[25] M. Kilic, E. Apaydin-Varol, A.E. Putun, Adsorptive removal of phenol from aqueous solutions on activated carbon prepared from tobacco residues: Equilibrium, kinetics and thermodynamics, J. Hazard. Mater 189 (2011) 397–403.

[26] H.T. Cordero, L.G.J. Aguilar, D.I.M. Castillo, V.H. Montoya, A.B. Petriciolet, M.A.M. Moran, Synthesis and adsorption properties of activated carbons from biomass of Prunus domestica and Jacaranda mimosifolia for the removal of heavy metals and dyes from water, Ind. Crops Prod. 42 (2013) 315–323.

[27] H. Marsh, F. Rodriguez-Reinoso, Activated Carbon, Elsevier Science & Technology Books, Amsterdam, 2006, pp. 1–420.

[28] D. Angin, T.E. Kose, U. Selengil, Production and characterization of activated carbon prepared from safflower seed cake biochar and its ability to absorb reactive dyestuff, Appl. Surf. Sci. 280 (2013) 705–710.

[29] Y.M. Hsieh, M.S. Tsai, Physical and chemical analyses of unburned carbon from oil-fired fly ash, Carbon 41 (2003) 2317–2324.

[30] R. Shawabkeh, M.J. Khan, A.A. Al-Juhani, H.I.A.A. Wahhab, I.A. Hussein, Enhancement of surface properties of oil fly ash by chemical treatment, Appl. Surf. Sci. 258 (2011) 1643–1650.

[31] A.L. Yaumi, I.A. Hussein, R.A. Shawabkeh, Surface modification of oil fly ash and its application in selective capturing of carbon dioxide, Appl. Surf. Sci. 266 (2013) 118–125.

[32] N. Rambabu, R. Azargohar, A.K. Dalai, J. Adjaye, Evaluation and comparison of enrichment efficiency of physical/chemical activations and functionalized activated carbons derived from fluid petroleum coke for environmental applications, Fuel Process. Technol. 106 (2013) 501–510.

[33] M. Balsamo, F.D. Natale, A. Erto, A. Lancia, F. Montagnaro, L. Santoro, Gasification of coal combustion ash for its reuse as adsorbent, Fuel 106 (2013) 147–151.

[34] P. Patnukao, A. Kongsuwan, P. Pavasant, Batch studies of adsorption of copper and lead on activated carbon from *eucalyptus camaldulensis* dehn. bark, J. Environ. Sci. 20 (2008) 1028–1034.

[35] Y. Jiang, E.R. Elswick, M. Mastalerz, Progression in sulfur isotopic compositions from coal to fly ash: Examples from single-source combustion in Indiana, Int. J. Coal Geol. 73 (2008) 273.

[36] M. Danish, R. Hashim, M.N.M. Ibrahim, O. Sulaiman, Effect of acidic activating agents on surface area and surface functional groups of activated carbons produced from *Acacia mangium* wood, J. Anal. Appl. Pyrolysis 104 (2013) 418–425.

[37] J. Kong, Q. Yue, L. Huang, Y. Gao, Y. Sun, B. Gao, Q. Li, Y. Wang, Preparation, characterization and evaluation of adsorptive properties of leather waste based activated carbon via physical and chemical activation, Chem. Eng. J. 221 (2013) 62–71.

[38] Y.S. Al-Degs, A. Ghrir, H. Khoury, G.M. Walker, M. Sunjuk, M.A. Al-Ghouti, Characterization and utilization of fly ash of heavy fuel oil generated in power stations, Fuel Process. Technol. 123 (2014) 41–46.

[39] M.H. Givianrad, M. Rabani, M.S. Tehrani, P.A. Azar, M.H. Sabzevari, Preparation and characterization of nanocomposite, silica aerogel, activated carbon and its adsorption properties for Cd(II) ions from aqueous solution, J. Saudi Chem. Soc. 17 (2013) 329–335.

[40] Y. Bulut, Z. Tez, Removal of heavy metals from aqueous solution by sawdust adsorption, J. Environ. Sci. 19 (2007) 160–166.

[41] D. Robati, Pseudo-second-order kinetic equations for modeling adsorption systems for removal of lead ions using multi-walled carbon nanotube, J. Nanostruct. Chem. 3 (2013) 55.

[42] D.D. Milenkovic, A.Lj. Bojic, V.B. Veljkovic, Ultrasound-assisted adsorption of 4-dodecylbenzene sulfonate from aqueous solutions by corn cob activated carbon, Ultrason. Sonochem. 20 (2013) 955–962.